Loss mechanisms in high efficiency polymer solar cells.

R. C. I. MacKenzie[1], V. S. Balderrama[2], S. Schmeisser[3], R. Stoof[4], S. Greedy[1], J. Pallarès[2], L. F. Marsal[2], A. Chanaewa[4], E. von Hauff[4]

[1] Faculty of Engineering, University of Nottingham, Nottingham NG7 2RD, United Kingdom

[2] Departament d'Enginyeria Electrònica Elèctrica i Automàtica, Universitat Rovira i Virgili, Avda. Països Catalans 26, 43007 Tarragona, Spain

[3] Institute of Physics, Albert-Ludwigs University of Freiburg, Hermann-Herder-Str. 3, 79104 Freiburg, Germany

[4] Physics Energy, Department of Physics and Astronomy, Amsterdam, Netherlands

Key words: polymer solar cell, organic photovoltaics, PTB7, impedance spectroscopy, intensity modulated photocurrent spectroscopy

We investigate performance losses and aging mechanisms in state-of-the-art PTB7:$PC_{70}BM$ solar cells. Inverted devices incorporating a vanadium pentoxide (V_2O_5) top contact have efficiencies of 8%. After aging the unencapsulated devices we observe no changes in the open circuit voltage (V_{oc}) or short circuit current (J_{sc}), however the fill factor (FF) drops from 0.7 to 0.61. An s-shape initially appears in the JV curve after aging, which can be reduced by cycling through the JV curve under illumination. We discuss this in context of the redox properties of V_2O_5. With impedance spectroscopy we demonstrate that changes to the contact interfaces are completely reversible and not responsible for the performance loss. Intensity Modulated Photocurrent Spectroscopy (IMPS) combined with device modelling reveals that the loss in FF is due to trap formation in the active layer. Additionally we observe that the performance of pristine devices is limited by optical absorption in the thin active layer and the build-up of space charge which hinders carrier extraction.

Introduction: Power conversion efficiencies of polymer solar cells have now surpassed 9 % [1,2,3,4]. The rapid increase in the performance is largely due to the development of novel donor-acceptor polymers with broad optical absorption [5]. State of the art power conversion efficiencies have been achieved using blends of poly[[4,8-bis[(2-ethylhexyl)-oxy]benzo[1,2-b:4,5-b']dithiophene-2,6-diyl][3-fluoro-2-[(2-ethylhexyl) carbonyl]thieno[3,4-b]thiophenediyl]] (PTB7)[6] and phenyl-C71-butyric acid methyl ester ($PC_{70}BM$) [2,7].

Despite promising results, the performance of PTB7:$PC_{70}BM$ solar cells is limited by the thin active layer3, carrier selectivity at the contacts [8], and rapid degradation of the active layer and contacts caused by exposure to ambient oxygen [9,10,11] and water vapour[12,]. Although inverted solar cell architectures have demonstrated high efficiencies combined with relatively good stability, age-induced performance loss in

high performance PTB7 solar cell architectures[2] has been reported, and the mechanisms are currently not well understood.

Identifying the origins of performance loss in any solar cells is challenging because it involves differentiating between interfacial phenomena and bulk properties [13]. Frequency resolved opto-electronic techniques such as impedance spectroscopy[14] and intensity modulated photocurrent spectroscopy (IMPS) [15] are useful in discriminating between electronic processes in the active layer and at contact interfaces, and correlating these with device performance. In this work, we combine these techniques with device modelling to identify key loss processes and aging mechanisms in state-of-the-art PTB7 based inverted solar cells incorporating a V_2O_5 hole transport layer. After prolonged exposure to ambient conditions no change in the open circuit voltage (V_{oc}) or short circuit current density (J_{sc}) were observed. An s-shape is initially observed in the JV characteristic, which can be reversed by cycling through the JV curve under illumination. Subsequently, a small drop in the fill factor (FF) from 0.7 to 0.61 was observed. With impedance spectroscopy, we demonstrate that changes to the device interfaces are completely reversible and that performance losses are due to degradation of the organic active layer. The IMPS analysis reveals age-related trap formation in the active layer. Interestingly, the high density of traps does not appear to have a significant effect on performance. We attribute this phenomenon to slow carrier thermalization times.

Experimental: The device structure is depicted in figure 1a. The PTB7:$PC_{70}BM$ active layer is sandwiched between an Indium tin oxide (ITO)/ poly[(9,9-bis(3-(N,N-dimethylamino)propyl)-2,7-fluorene)-alt-2,7-(9,9–dioctylfluorene)] (PFN) [16] electron extracting contact and a V_2O_5 [17,18,19,20,21]/Ag hole extracting contact. The PFN and active layer were deposited using spin coating, while the V_2O_5 and silver (Ag) were deposited using thermal evaporation. The relative energy levels of the layers are shown in fig. 1b [2,22]. Impedance and IMPS measurements were carried out using a Metrohm Autolab. JV measurements were carried out using a Keithley 2401 source measurement unit in combination with a solar simulator SS80 (Photo Emission Tech, Inc.). Full details of the fabrication and measurement process can be found in the supplementary information.

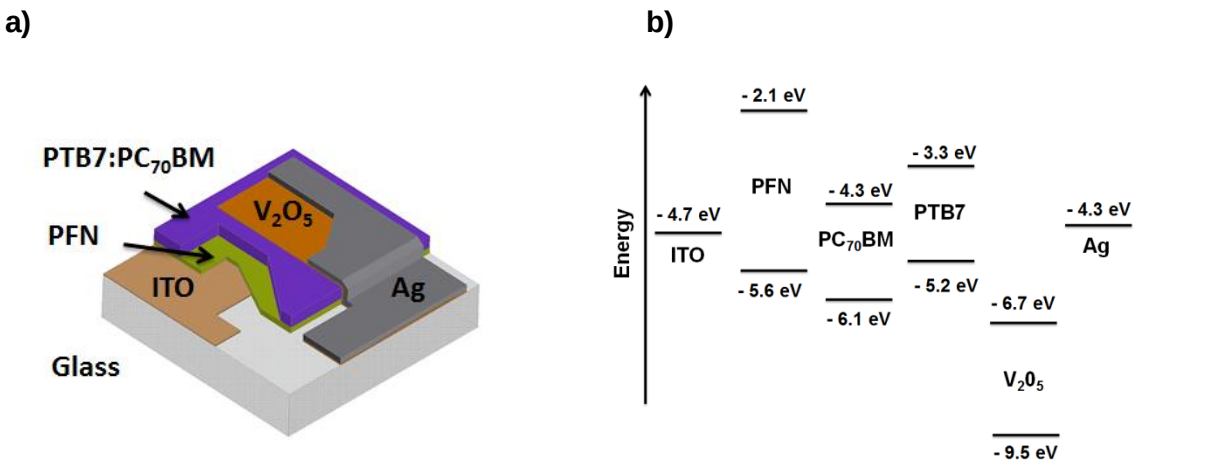

Figure 1 a) the solar cell architecture used in this study b) relative energy positions of the contact materials (ITO, PFN, V_2O_5 and Ag) and active layer (PTB7 and $PC_{70}BM$).

Results: A typical light JV curve for a fresh PFN/PTB7:$PC_{70}BM$/V_2O_5/Ag device is shown in Fig. 2 (red dots). This cell has an efficiency of 8 % (J_{sc} = 16.7 mA/cm^2, V_{oc} = 0.69 V and fill factor (FF) = 0.7). The black symbols (Fig. 2) represent the JV curve of the same device after it has been exposed to air for four weeks (ISOS standard D-1 [23]). It can be seen that after exposure to air, both J_{sc} and V_{oc} remain constant, but FF is reduced to 0.61. We observe an s-shape initially in the JV characteristics after ageing. The s-shape can be eliminated by cycling through the JV curve under illumination.

Previously S-shaped JV curves have been attributed to a reduction in charge extraction efficiency [24,25,26,27,28] due to the formation of an extraction barrier at the contacts [29,30,31]. Interesting, we also note that when the aged device is successively cycled through the JV curve under illumination, the S-shape is reduced (Fig. 2, grey symbols) and after 100 cycles the JV curve fully recovers, except for a drop in FF to 0.61. This suggests that JV cycling under light exposure reduces the height of an extraction barrier within the device. Other reports have shown that PTB7:$PC_{70}BM$ blends are highly sensitive to photo-oxidation [9,10]. The fact that V_{oc} and J_{sc} do not change with aging, suggests that the V_2O_5 hole collection layer is at least partially encapsulating the active layer from irreversible degradation [32]. We attribute both the stability of the device architecture, as well as the recovery of the JV characteristics after aging to the redox properties of V_2O_5.

V_2O_5 is a well-known oxidizing agent, and oxygen vacancies in V_2O_5 are easily induced [12,33,34,35,36] via annealing [35,36] and environmental exposure [12,22]. The

reduction of V^{5+} to lower oxidation states has been correlated with a decrease in the work function of V_2O_5 films [22], which would represent an extraction barrier for holes from the solar cell. When the device is illuminated, however, electron injection from the conduction band of the V_2O_5 into the HOMO of the donor molecule subsequently re-oxidizes the V_2O_5 thereby reducing the extraction barrier. Teran-Escobar et al. recently reported on a similar phenomenon, and correlated the age and oxidation state of solution deposited V_2O_5 layers with the quality of the JV characteristics of P3HT:PCBM solar cells [12]. The complete reversibility of the s-shape in the JV of our solar cells compared to partial recovery observed in [12] can be due to the difference in the properties and quality of thermally evaporated versus solution processed V_2O_5 layers. These results demonstrate the potential of achieving high stability in organic photovoltaics via chemical control [37] of the contact interfaces to tune extraction barriers.

To demonstrate the stability of the device interfaces and confirm that performance loss after aging is only related to changes in the active layer, we apply impedance spectroscopy. Impedance spectroscopy has previously been widely applied to study recombination, transport and carrier extraction barriers in organic solar cells [24,30,31,38,39,40]. Measurements were performed under illumination on the pristine device (fresh), and on the degraded device after the S-shape had been eliminated from the JV (aged).

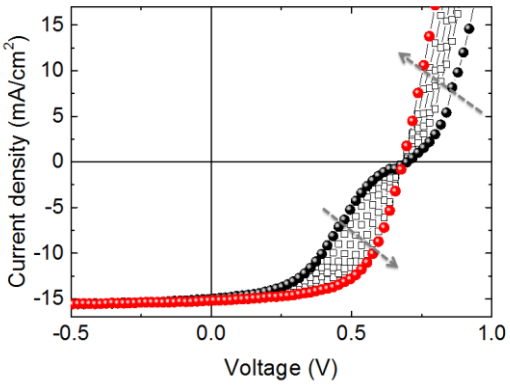

Figure 2 JV characteristics of a solar cell exposed to ambient conditions for four weeks. The black symbols show the initial JV curve, and gray symbols and arrows depict successive JV

cycles to recover the solar cell performance. The red symbols show the JV characteristics after 100 sweeps.

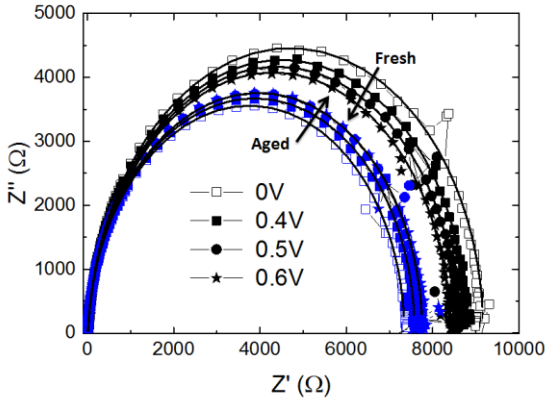

Figure 3 Cole-Cole plots for the device under illumination before (black) and after (blue) aging are shown for applied DC voltages of 0 V, 0.4 V, 0.5 V and 0.6 V.

Fig. 3 shows the Cole-Cole representation of the impedance data taken under illumination from the fresh solar cell (black) and after (blue) aging. It can be seen that both the real (Z') and imaginary (Z'') impedance values are slightly lower for the aged device. Furthermore, it can be seen that the impedance increases minimally with applied DC voltage after aging. Interestingly, we do not observe features in the impedance spectra which are characteristic of contact corrosion impeding charge extraction, i.e. peaks in the dielectric loss spectra and/or the emergence of new, high frequency features [24,31,41], indicating that after voltage cycling the device, the extraction barrier resulting in the S-shape is eliminated.

To better understand the impedance spectra, we fit the data with an equivalent circuit model consisting of 3 resistor-capacitor (RC) elements [38]. The solid lines in fig. 3 show the fits. The details of this procedure can be found in the supporting information (SI). This allowed us to correlate changes in the impedance spectra before and after aging with the opto-electronic response of physical sites in the solar cell, i.e. the contact interfaces and the bulk active layer [38,42]. From this analysis, we observe a decrease in the series resistance of the device after aging which we attribute to the V_2O_5 layer. Additionally there is a decrease in the resistance of the RC element associated with the response of the active layer. We do not observe any age-induced changes in the circuit elements associated with the contact interfaces. This suggests that changes in device response after aging are only related to the active layer and

that changes to the contact interfaces in this device architecture are completely reversible.

To gain insights into degradation of the active layer resulting in the decrease in the FF we employ IMPS. IMPS has been widely applied to study electrochemical systems [15] such as dye sensitised solar cells [43], but rarely to study organic photovoltaics [44,45,46,47]. In this measurement a small optical AC perturbation is superimposed on the background light intensity, causing periodic variations in carrier density. By monitoring the changes in the photocurrent collected at the contacts as a function of light modulation, transient phenomena such as trapping, recombination and charge transfer at material interfaces can be probed as a function of carrier density. The resulting change in the photocurrent density (J) is fit with equation,

$$J(t) = Jexp(i\omega t - \Phi) \quad (1)$$

where J represents the magnitude of the change in photocurrent, and Φ represents the phase shift between the light modulation and the current response.

In the following measurements, the cell was kept at short circuit and illuminated with a red LED (627 nm) with background bias light intensities of 50 mW/cm^2, 100 mW/cm^2, 150 mW/cm^2 and 200 mW/cm^2.

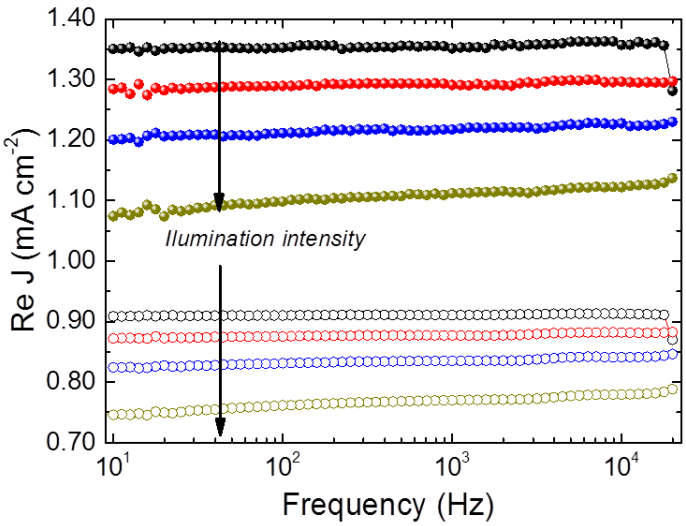

Figure 4 Re(J) vs. frequency before (closed symbols) and after (open symbols) aging for illumination intensities of 50 mW/cm^2, 100 mW/cm^2, 150 mW/cm^2 and 200 mW/cm^2 with a red LED (627 nm). The arrows indicate increasing background light intensity.

Figure 4 depicts the real (Re) component of J vs. frequency as a function of background light intensity, measured before (closed symbols) and after aging (open symbols). Re(J) decreases with increasing illumination intensity. At higher light intensities carrier density is higher and recombination increases, and the sinusoidal perturbation produces less change in the current density collected at the contacts. In addition, a weak positive dependence of Re(J) on frequency is observed. A comparison of the spectra reveals that the optical perturbation produces less change in J after aging.

a) **b)**

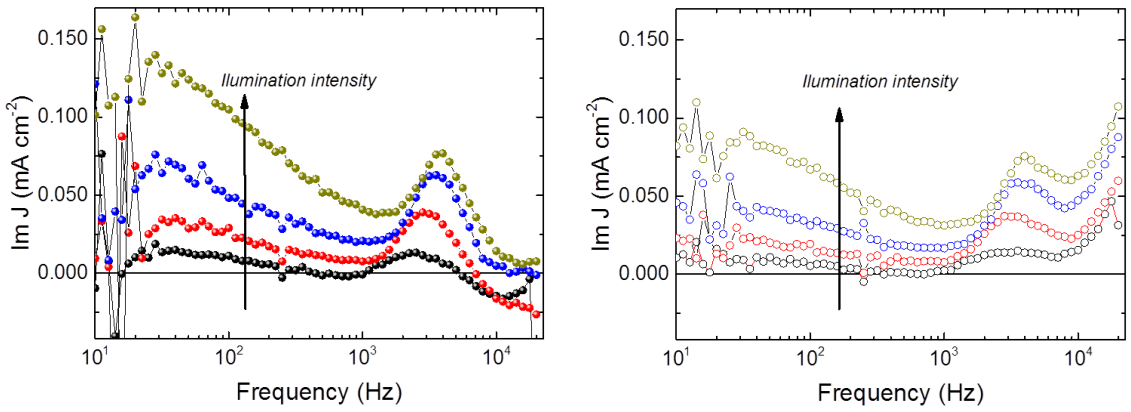

Figure 5 Im(J) spectra a) before and b) after aging at illumination intensities of 50 mW/cm^2, 100 mW/cm^2, 150 mW/cm^2 and 200 mW/cm^2 with a red LED (623 nm).

The imaginary component of J, Im(J), is plotted in Fig. 5 a) before and b) after aging. Im(J) reflects how the generated photocurrent leads or lags the modulation in light intensity. The trend of the Im(J) spectra of the solar cell before and after aging are very comparable, except in the high frequency regime. Im(J) values are more than 10 times lower than Re(J) values, indicating that the phase shift between photogeneration and charge extraction in the device is small. Interestingly, Im(J) is mostly positive, particularly at low frequencies and with increasing light intensity. This indicates that the maximum in extracted photocurrent precedes that of the photoflux, i.e. the device produces a maximum current before the modulated light intensity peaks. Im(J) decreases gradually between 10 Hz and 1 kHz, before peaking around 3 kHz. Before aging, at frequencies above 4 kHz, the Im(J) spectra decreases and becomes negative. After aging the device, however, Im(J) increases at higher frequencies.

Previously, positive values of Im(J) have been attributed to degradation-induced trap formation [46]. However, we would not expect to see this in fresh, high efficiency devices. Furthermore, the gradual drop in Im(J) and the peak at 4kHz have not been previously reported. Difficulties in interpreting IMPS data from organic photovoltaics due to the complex interfacial phenomena combined with wide range of time scales for key electronic processes have limited its application in the field to date [45]. Therefore, to analyse our results, we developed a Shockley-Read-Hall based [48,49], drift-diffusion model to quantify the features in the spectra.

The model uses an effective medium approximation to describe the electrical characteristics of the device [50]. The model solves Poisson's equation, the electron/hole drift diffusion equations and the carrier continuity equations in 1D from the cathode to the anode. The energetic distribution of trap states in energy space is assumed to be exponential and the optical profile within the device is calculated using the transfer matrix method (see SI for details).

The device model was fit self-consistently to both the illuminated JV curve, and two cycles of the IMPS response of the device, at 39 Hz and at 2818.4 Hz. In order to keep the interpretation of the results as simple as possible and reduce the number of fitting parameters, the model parameters were kept symmetric. Once the model was calibrated to the experimental data, we asked the model to predict the shape of the Re(J) and Im(J) spectra from 10 Hz - 5 kHz (fig. 6). A comparison between the experimental (fig. 4) and simulated (fig. 6 a)) Re(J) spectra reveals the same trend; a gradual increase in Re(J) with frequency, and a decrease in signal with increasing light intensity.

In the case of Im(J), experimental (fig. 5) and simulated (fig. 6 b) spectra both show a positive photocurrent. This indicates that when responding to a sinusoidal optical excitation, the device reaches its maximum efficiency and produces most current before the light intensity is at its maximum. This is a counterintuitive effect, and is not expected in high efficiency devices at low frequencies. For frequencies which approach the DC case, it would be expected that changes in the light intensity result in immediate changes in the photocurrent. Time delays between optical modulation and photocurrent response at low frequencies indicates loss processes even in the fresh devices. The increase in the magnitude of Im(J) with increasing light intensity suggests processes dependent on illumination and/or charge density.

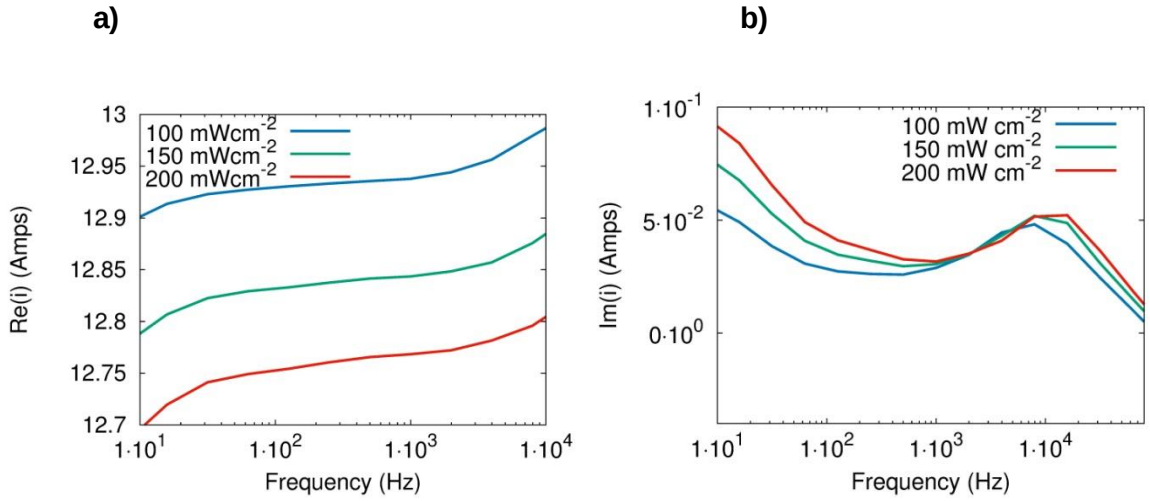

Figure 6 Simulated (a) Re J and (b) Im J response of the device plotted as a function of light intensity.

Increasing the carrier density in low mobility organic materials is expected to lead to the build-up of space-charge. With our model we were able to produce a positive Im(J) current at low frequencies by using parameters which encouraged the formation of non-uniform and transient spatial distributions of charge within the device, resulting in band bending which hinders charge extraction [15]. This resulted in a peak in photocurrent generation and device efficiency before the modulated light reached its maximum intensity. The effect could be turned on by increasing the energetic distribution of trap states while keeping the recombination rate low. The effect could be turned off by artificially increasing the permittivity of the material in the simulation to prevent band bending (see SI).

We now consider the optical properties of the organic active layer as a function of light intensity. Im(J) decreases between 10 Hz to 3 kHz (Fig. 5). Interestingly, we were unable to reproduce this by varying the electrical parameters in the model alone. Furthermore, we were unable to self-consistently fit the JV curve while simultaneously producing the experimentally observed peak above 1 kHz in the Im(J) spectra. In order to self-consistently reproduce all the experimental trends in the Im(J) spectra with the model, we had to allow the optical absorption of the active layer to decrease as light intensity was increased, simulating reversible optical bleaching. Under increasing illumination intensity, bleaching of the active layer occurs as higher energy states are filled with charge, depleting the ground state and making the promotion of further carriers to higher states unlikely. Once easily excitable charge occupies these higher states, α decreases.

We modeled this effect by reducing the optical absorption coefficient α of the active layer as a function of local free carrier density,

$$\alpha(x) = \alpha_0(x) + \rho\left(n_f^0(x)\, p_f^0(x) - n_f(x)\, p_f(x)\right) \quad (2)$$

where $n_f{}^o(x)$ and $p_f{}^o(x)$ are spatially dependent density of free carriers at equilibrium in the dark, $n_f(x)$ and $p_f(x)$ are the density of free carriers out of equilibrium.

We then examined the distinctive peak in the Im(J) spectra (fig. 5) at ~ 3 kHz. The position of this peak can be shifted by altering the carrier capture and recombination cross sections. This peak is still observed even if the permittivity of the medium is increased to a very high value to turn off electrostatic effects and band bending. We explain this effect by considering that increasing the frequency of light modulation leads to increasing lag in the carrier recombination with respect to carrier generation, as the occupation of trap states is retarded at higher frequencies. As the frequency of light modulation approaches 3 kHz the trapped carrier population is 180° out of phase with carrier generation, resulting from carrier recombination being faster than carrier thermalization (see SI).

We finally turn our attention to the differences in the high frequency behaviour of the Im(J) spectra before and after aging. Before the device is aged (fig. 5 a) and 6 b)), Im(J) values continually decrease at frequencies above 3 kHz and become negative. Negative Im(J) values occur when photogenerated charge cannot be transported to the contacts as fast as the optical field is changing. Furthermore, because the optical field is changing so fast, there is not enough time during the IMPS oscillation to allow a build-up of space charge to hinder extraction. Thus a negative imaginary IMPS signal indicates that the transit time of the carriers is longer than the period of the modulating light. After aging the device (fig. 4 b)) Im(J) continually increases at higher frequencies. This behaviour could be reproduced in the model by increasing the density of trap states from $5\text{x}10^{25}$ m^{-3} eV^{-1}. to $5\text{x}10^{26}$ m^{-3} eV^{-1} (Fig. 7), but not by changing recombination rates or carrier mobility values.

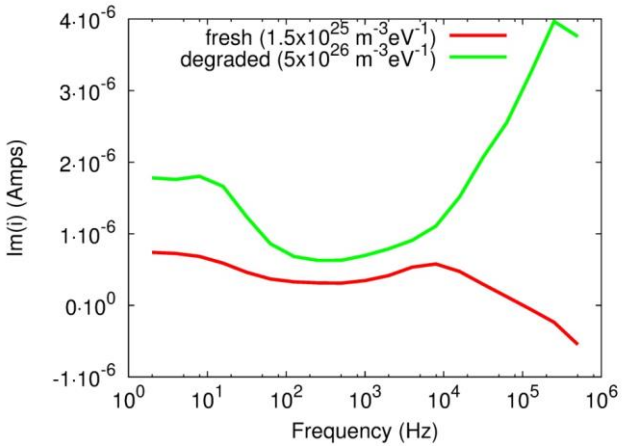

Figure 7 The simulated IMPS spectra of the fresh device (red line) and of a device with an increased number of trap states (green line).

Lastly it should be noted that none of the features in the Im(J) spectra could be reproduced by introducing extraction barriers at the device interfaces. This is in agreement with the results from the impedance analysis. Based on the impedance and IMPS results, the slight loss in FF after ambient exposure is attributed to low density trap formation in the organic active layer.

We are able to apply IMPS together with device modelling to quantify loss processes in high efficiency, pristine PTB7:$PC_{70}BM$ solar cells. On the one hand, low carrier mobility, likely in the polymer phase, results in the build-up of space charge in the active layer, preventing the extraction of charge from the device. The poor transport properties of PTB7 layers is a reason why optimized solar cells based on PTB7 employ extremely thin active layers[2,8]. We confirm, however, that the photocurrent in the device is ultimately determined by limitations in the optical absorption of these thin active layers[3]. We note that the effects are minimal under lower illumination (very low Im(J) values), but become increasingly apparent as the intensity is increased.

After aging the device, the trap density within the active layer is found to increase by over an order of magnitude. Interestingly this does not affect carrier mobility values or recombination rates, and as a result, the photocurrent does not decrease. This could be due to the charge carrier capture cross section being over three orders of magnitude smaller than for a material system with molecularly ordered domains such as P3HT:PCBM [51]. The high efficiencies achieved with PTB7:$PC_{70}BM$ blends have been attributed to minimizing the domain sizes of the polymer and fullerene phases to facilitate efficient charge transfer [52]. Further, the PTB7:$PC_{70}BM$ active layer is kept thin (<100 nm) to minimize non-geminate

recombination losses in the amorphous polymer phase [53,54]. In contrast, solar cells based on P3HT:PCBM do not demonstrate pronounced dependence on the thickness of the active layer 8.

The underlying molecular mechanisms related to degradation of the PTB7:$PC_{70}BM$ blend are not yet well understood [55], in contrast to the well-studied P3HT:PCBM system [56], Recently Razzell-Hollis et al. [9] applied Raman spectroscopy to monitor molecular level changes in PTB7:PC70BM blends after photodegradation. They found that photo-oxidation is a two-step process, and applied DFT to find that hydroxyl formation on the BDT unit was linked as a probable cause connected to final, irreversible degradation. Cox et al. [10] used frequency modulated electrostatic force microscopy on PTB7:$PC_{70}BM$ blends and showed that photodegradation results in local variations in the measured surface potential of the blend on the scale of 40 nm. The DIO additive used in high efficiency blends stabilised the blends against degradation, and prevented larger scale damage. Based on these results, we attribute the observed performance loss in our PTB7:$PC_{70}BM$ solar cells to molecular scale changes to the polymer backbone, and not due to larger scale morphological changes of the blend.

Conclusions

We investigate loss mechanisms in efficient inverted PTB7:$PC_{70}BM$ solar cells. Upon exposure to ambient conditions for several weeks, an s-shape emerges in the JV curve. Cycling through the JV curve under illumination leads to reduction of the s-shape and recovery of the JV curve. No losses in V_{oc} or J_{sc} due to aging were observed, however the FF drops from 0.7 to 0.61. Both impedance spectroscopy and IMPS demonstrated that after JV cycling there was no significant extraction barrier present in the device, indicating that changes to the contact interfaces are completely reversible. By applying a Shockley-Read-Hall drift-diffusion model together with IMPS measurements, we investigate processes related to performance loss in the active layer. We demonstrate that the intensity-dependent positive Im(J) response of the IMPS spectra at low frequencies indicates reversible optical bleaching of the thin active layer as well as band bending effects. Traps are formed in the active layer upon aging, however, they do not significantly decrease device performance. We attribute this to a slow carrier thermalization rate in the PTB7 material system. These results reveal that key performance limiting mechanisms in state of the art organic solar cells.

Acknowledgements

S.S, A.C and E.v.H. acknowledge support from Fraunhofer Institute of Solar Energy Systems, and financial support from the German Science Foundation (DFG) and the Foundation for Fundamental Research on Matter (FOM) (V0714M-13MV60) from the Netherlands Organization for Scientific Research (NWO). V.B, J.P and L.F.M thank the Spanish Ministry of Economy and Competitiveness TEC2012-34397, Catalan Government AGAUR 2014SGR1433 and the ICREA Academia Award.

1 M. A. Green, K. Emery, Y. Hishikawa, W. Warta and E. D. Dunlop, Prog. Photovolt: Res. Appl., 2014, 22, 701.

2 Z. He, C. Zhong, S. Su, M. Xu, H. Wu and Y. Cao, Nature Photonics, 2012, 6, 593.

3 Y. Liu, J. Zhao, Z. Li, C. Mu, W. Ma, H. Hu, K. Jiang, H. Lin, H. Ade, H. Yan, Nature Comm. 2014, 5, 5293

4 I. Etxebarria, J. Ajuria, R. Pacios, Organic Electronics, 2015, 19, 34.

5 G. Li, R. Zhu and Yang Yang, Nature Photonics, 2012, 6, 153.

6 Y. Liang, Z. Xu, J. Xia, S.-T. Tsai, Y. Wu, G. Li, C. Ray and Luping Yu, Adv. Mater., 2010, 22, E135.

7 L. Lu and L. Yu, Adv. Mater. 2014, 26, 4413.

8 A. Guerrero, N. F. Montcada, J. Ajuria, I. Etxebarria, R. Pacios, G. Garcia-Belmonte and E. Palomares, J. Mater. Chem. A, 2013, 1, 12345.

9 J. Razzell-Hollis, J. Wade, W. C. Tsoi, Y. Soon, J. Durrant and J.-S. Kim, J. Mater. Chem. A, 2014, 2, 20189.

10 P. A. Cox, D. A. Waldow, T. J. Dupper, S. Jesse, D. S. Ginger, ACS Nano, 2013, 7, 10405

11 E. A.A. Arbab, B. Taleatu, G. T. Mola, Journal of Modern Optics, 2014, 61, 1749

12 P. Romero-Gomez, R. Betancur, A. Martinez-Otero, X. Elias, M. Mariano, B. Romero, B. Arredondo, R. Vergaz, J. Martorell, Sol. Energy. Mater. Solar Cells, 2015, 37, 44

13 M. Jorgensen, K. Norrman, S. Gevorgyan, T. Tromholt, B. Andreasen, F. C. Krebs, Adv. Mater. 2012, 24, 580

14 J. R. Macdonald, Annals of Biomedical Engineering, 1992, 20, 289.

15 E. A. Ponomarev, L.M. Peter, J. Journal of Electroanalytical Chemistry, 1995, 396, 219.

16 F. Huang, H. B. Wu, D. L. Wang, W. Yang and Y. Cao, Chem. Mater., 2004, 16, 708.

17 G. Teran-Escobar, J. Pampel, J. M. Caicedo, M. Lira-Cantu, Energy and Environmental Science, 2013, 6, 3088.

18 M. Terai, K. Fujita and T. Tsutsu, Jpn. J. Appl. Phys., 2005, 44, L 1059.

19 K. Zilberberg, S. Trost, H. Schmidt and T. Riedl, Adv. En. Mater., 2011, 1, 377.

20 M. G. Helander, Z. B. Wang, M. T. Greiner, J. Qiu and Z. H. Lu, Appl. Phys. Lett., 2009, 95, 083301

21 V. Shrotriya, G. Li, Y. Yao, C.-W. Chu and Y. Yang, Appl. Phys. Lett., 2006, 88, 073508.

22 J. Meyer, K. Zilberberg, T. Riedl and A. Kahn, J. Appl. Phys., 2011, 110, 033710.

23 M. Reese et al., Sol. Mater. Sol. Cells, 2011, 95, 1253.

24 M. Glatthaar, M. Riede, N. Keegan, K. Sylvester-Hvid, B. Zimmermann, M. Niggemann, A. Hinsch, A. Gombert, Sol. Energy Mater. Sol. Cells, 2007, 91, 390.

25 A. Wagenpfahl, D. Rauh, M. Binder, C. Deibel and V. Dyakonov, Phys. Rev. B, 2010, 82, 115306

26 W. Tress, K. Leo and M. Riede, Adv. Funct. Mater., 2011, 21, 2140.

27 B. Y. Finck and B. J. Schwartz, Appl. Phys. Lett., 2013, 103, 053306.

28 L. Sims, Ulrich Hörmann, R. Hanfland, R. C.I. MacKenzie, F. R. Kogler, R. Steim, W. Brütting, P. Schilinsky, Organic Electronics, 2014, 15, 2862.

29 E. Voroshazi, B. Verreeta, A. Buric, R. Müller, D. Di Nuzzo and P. Heremans, Organic Electronics, 2011, 12, 736.

30 B. Ecker, J. Nolasco, J. Pallarés, L. Marsal, J. Posdorfer, J. Parisi and E. von Hauff, Adv. Funct. Mat., 2011, 21, 2705.

31 B. Ecker, J. Posdorfer and E. von Hauff, Sol. Energy Mat. Sol. Cells, 2013, 116, 176.

32 T. Yanagidate, S. Fujii, M. Ohzeki, Y. Yanagi, Y. Arai, T. Okukawa, A. Yoshida, H. Kataura, Y. Nishioka, Japanese Journal of Applied Physics, 2014, 53, 02BE05

33 R. Rambez, B. Casal, L. Utrera and E. Ruiz-Hitzky, J. Phys. Chem. 1990, 94, 8960.

34 Q.-H. Wua, A. Thissen, W. Jaegermann and M. Liu, Appl. Surf. Sci., 2004, 236, 473.

35 D. S. Su and R. Schlögl, Catalysis Letters, 2002, 83, 115.

36 S. Guimond, J. M. Sturm, D. Göbke, Z. Romanyshyn, M. Naschitzki, H. Kuhlenbeck and H.-J. Freund, J. Phys. Chem. C, 2008, 112, 11835.

37 S. R. Cowan , P. Schulz , A. J. Giordano , A. Garcia , B. A. MacLeod, S. R. Marder , A. Kahn , D. S. Ginley , E. L. Ratcliff, D. C. Olson, Adv. Funct. Mater., 2014, 24, 4671.

38 A. Guerrero, N. F. Montcada, J. Ajuria, I. Etxebarria, R. Pacios, G. Garcia-Belmonte and E. Palomares, J. Mater. Chem. A, 2013, 1, 12345.

39 B. Ecker, R. Steim, H. J. Egelhaaf, J. Parisi and E. von Hauff, J. Phys. Chem., 2012, 116, 16333.

40 J. Bisquert, L. Bertoluzzi, I. Mora-Sero, G. Garcia-Belmonte, J. Phys. Chem. C, 2014, 118, 18983.

41 B. Ecker, R. Steim, H. J. Egelhaaf, J. Parisi and E. von Hauff, J. Phys. Chem., 2012, 116, 16333.

42 D. A. Harrington ,P. van den Driessche, Electrochimica Acta, 2011, 56 8005.

43 P. E. de Jongh and D. Vanmaekelbergh, Phys. Rev. Lett, 1996, 77, 3427.

44 T. Oekermann, D. Schlettwein, N. I. Jaeger, J. Phys. Chem. B, 2001, 105, 9524.

45 P.M. DiCarmine, O.A. Semenikhin, Electrochimica Acta, 2008, 53, 3744.

46 Y. T. Set, M. D. Heinemann, E. Birgersson and Joachim Luther, J. Phys. Chem. C, 2013, 117, 7993.

47 S. Cho, K.-D. Kim, J. Heo, J. Y. Lee, G. Cha, B. Y. Seo, Y. D. Kim, Y. S. Kim, S.-y. Choi and D. C. Lim, Scientific Reports, 2014, 4, 4306

48 W. Shockley and W. T. Read. Phys. Rev., 1952, 87, 835.

49 R. C. I. MacKenzie, C. G. Shuttle, M. L. Chabinyc, and J. Nelson. Advanced Energy Materials, 2012, 2, 662.

50 L. J. A. Koster, E. C. P. Smits, V. D. Mihailetchi, and P. W. M. Blom. Phys. Rev. B, 2005, 72, 085205.

51 R. C. I. MacKenzie , C. G. Shuttle, M. L. Chabinyc, J. Nelson, Adv. Energy. Mater., 2012, 6, 662.

52 B. A. Collins, Z. Li, J. R. Tumbleston, E. Gann, C. R. McNeill, H. Ade, Adv. Energ. Mater., 2013, 3, 65.

53 M. R. Hammond, R. J. Kline, A. A. Herzing, L. J. Richter, D. S. Germack, H.-W. Ro, C. L. Soles, D. A. Fischer, T. Xu, L. Yu, M. F. Toney, D. M. DeLongchamp, ACS Nano, 2011, 5, 8248.

54 Y. Liu, J. Zhao, Z. Li, C. Mu, W. Ma, H. Hu, K. Jiang, H. Lin, H. Ade, H. Yan, Nature Comm. 2014, 5, 5293

55 S. Shah, R. Biswas, J. Phys. Chem. C, 2015, 119, 20265

56 F. Deschler, A. De Sio, E. von Hauff, P. Kutka, T. Sauermann, H.-J. Egelhaaf, J. Hauch, E. Da Como, Adv. Funct. Mater., 2012, 22, 1461